J Neurophysiol. Author manuscript; available in PMC 2016 October 06.

Published in final edited form as:

J Neurophysiol. 2006 May ; 95(5): 2933–2946. doi:10.1152/jn.01296.2005.

Nonlinear Information Processing in a Model Sensory System

Maurice J. Chacron

Department of Zoology, University of Oklahoma, Norman, Oklahoma

Abstract

Understanding the mechanisms by which sensory neurons encode and decode information remains an important goal in neuroscience. We quantified the performance of optimal linear and nonlinear encoding models in a well-characterized sensory system: the electric sense of weakly electric fish. We show that linear encoding models generally perform better under spatially localized stimulation than under spatially diffuse stimulation. Through pharmacological blockade of feedback input and spatial saturation of the receptive field center, we show that there is significantly less synaptic noise under spatially diffuse stimuli as compared with spatially localized stimuli. Modeling results suggest that pyramidal cells nonlinearly encode sensory information through shunting in their dendrites and clarify the influence of synaptic noise on the performance of linear encoding models. Finally, we used information theory to quantify the performance of linear decoders. While the optimal linear decoder for spatially localized stimuli could capture 60% of the information in pyramidal cell spike trains, the optimal linear decoder for spatially diffuse stimuli could only capture 40% of the information. These results show that nonlinear decoders are necessary to fully access information in pyramidal cell spike trains, and we discuss potential mechanisms by which higher-order neurons could decode this information.

INTRODUCTION

The discovery of behaviorally relevant neural codes remains an important goal in sensory physiology (Rieke et al. 1996). Progress toward this goal requires determining the relation between behaviorally relevant input signals and the patterns of action potentials that they elicit from sensory neurons, the encoding process, as well as subsequent decoding of these patterns by higher brain centers. The discovery of such codes is complicated by the fact that the same stimulus pattern will not always give rise to the same spike train (Mainen and Sejnowski 1995) and that behaviorally relevant input signals are often unknown (Krahe and Gabbiani 2004). Moreover, the mechanisms by which sensory neurons encode information can be very different from the optimal algorithms used to decode this information (Rieke 1992; Treves 1997): information encoded nonlinearly can sometimes be decoded linearly (Rieke et al. 1996). Furthermore, whereas neurons are clearly nonlinear, linear models can often adequately describe the neural encoding process for weak (i.e., low intensity) sensory stimuli (Roddey et al. 2000).

Address reprint requests and other correspondence to: Dept. of Zoology, University of Oklahoma, 730 Van Vleet Oval, Norman, OK, 73019 mauricejchacron@yahoo.ca.

On the other hand, it is commonly assumed that neural responses can be decoded linearly (Rieke et al. 1996). Several studies have shown that this is not always the case and that nonlinear decoders are necessary for strong (i.e., high intensity) stimuli in the visual (Passaglia and Troy 2004) and auditory systems (Marsat and Pollack 2004, 2005). This was done with information theory (Cover and Thomas 1991; Shannon 1948). Mutual information rates can be directly estimated from the probability of obtaining various neural responses (De Ruyter van Steveninck et al. 1997; Reinagel and Reid 2000; Strong et al. 1998). This direct method makes no assumptions about the neural code and is exact in principle (Borst and Theunissen 1999). It, however, does not give much insight as to the mechanisms by which neurons process information and furthermore requires large data sets. For this reason, investigators have turned to other techniques that make assumptions on the nature of the code. One such approach is to reconstruct the stimulus from the neural response using Wiener kernels: the indirect method (Gabbiani 1996; Rieke et al. 1996). Typically, only the first-order (linear) kernel is used (Gabbiani 1996; Theunissen et al. 1996; Wessel et al. 1996), and the amount of information thus estimated will in general be a lower bound on the rate of information transmitted by the neuron. A direct comparison between the mutual information rate estimates from the indirect and direct methods will yield an estimate of the relative amount of information that can be decoded linearly and thus quantify the performance of optimal linear decoders.

From the arguments presented in the preceding text, it seems that strong stimuli might require both nonlinear encoding and decoding mechanisms, whereas linear encoding and decoding might be sufficient for weak sensory stimuli. To determine the nature of the nonlinearities elicited by strong stimuli, we quantified the performance of nonlinear encoding and decoding models for pyramidal neurons in the electrosensory lateral line lobe (ELL) of weakly electric fish using both weak and strong stimuli. Electroreceptor afferents detect amplitude modulations of the animal's self-generated electric field and relay this information to pyramidal cells in the electrosensory lateral line lobe (ELL) (Turner et al. 1999). There are large heterogeneities present in the pyramidal cell population: receptive field organization, apical and basal dendritic morphology, the tendency to fire bursts of action potentials, adaptive cancellation of redundant stimuli through synaptic plasticity, and sensitivity to the stimulus' spatial extent were all found to be highly correlated with baseline firing rate (Bastian and Courtright 1991; Bastian and Nguyenkim 2001; Bastian et al. 2002, 2004; Chacron et al. 2005c). The baseline firing rate is thus a convenient quantifier of ELL pyramidal cell heterogeneities. There are two classes of pyramidal cells: E-cells, or basilar pyramidal cells, are excited by increases in the EOD amplitude while I-cells, or nonbasilar pyramidal cells, are inhibited by increases in the EOD (Maler 1979; Maler et al. 1981; Saunders and Bastian 1984). Furthermore, pyramidal cells found most superficially in the ELL have low firing rates and large apical dendritic trees while cells found more deeply have high firing rates and small apical dendritic trees (Bastian and Courtright 1991; Bastian and Nguyenkim 2001).

Previous studies in a related fish species have estimated lower bounds on the rate of information transmission and thus shown that receptor afferents were adept at encoding the detailed time course of the stimulus (Gabbiani et al. 1996; Kreiman et al. 2000; Metzner et al. 1998; Wessel et al. 1996), whereas pyramidal cells responded only to specific features of

the stimulus (Gabbiani et al. 1996; Metzner et al. 1998). Behaviorally relevant stimuli fall within two broad categories: prey stimuli that impinge only on part of pyramidal cell receptive fields are spatially localized and inherently weak (Nelson and MacIver 1999), whereas electrocommunication stimuli that impinge on the entire body surface of the animal are spatially diffuse and stronger (Zupanc and Maler 1993). It was also found that pyramidal cells could switch their frequency tuning in a behaviorally relevant manner based on the stimulus' spatial extent (Chacron et al. 2003, 2005c). All but one of these studies were conducted assuming a linear decoder, and that study (Metzner et al. 1998) found that a particular nonlinear decoder did not significantly improve the information rate. However, because nonlinear encoding and decoding mechanisms have been found in the visual, auditory, and cercal systems, it is probably safe to assume that they are present in the electrosensory system as well. To gain understanding as to the nature of possible nonlinear mechanisms of information transmission in the electrosensory system, we assessed the performance of linear encoding models relative to the maximum theoretically achievable performance of nonlinear models for both receptor afferents and pyramidal cells under different behaviorally relevant stimulation geometries. This was done to gain insights as to how information transmitted by electroreceptor afferents is encoded by their postsynaptic targets: pyramidal cells. We also computed mutual information rates of pyramidal cells using both the direct and indirect methods to gauge the performance of linear decoders. A combination of electrophysiological, pharmacological, and modeling reveals the nonlinear mechanism used by pyramidal cells for encoding sensory stimuli. Our results show that information encoded in a nonlinear manner must also be decoded nonlinearly and we discuss potential decoding mechanisms by higher brain centers. Finally, we show in an APPENDIX that spike timing jitter does not significantly distort the spike-triggered averages of both receptor afferents and pyramidal cells.

METHODS

The weakly electric fish *Apteronotus leptorhynchus* was used exclusively in this study. Animals were housed in groups of 3–10 in 150-l tanks, temperature was maintained between 26 and 28°C. Experiments were performed in a 30 × 30 × 10-cm-deep Plexiglass aquarium with water recirculated from the animal's home tank. Artificial respiration was achieved with a continuous flow of water at a rate of 10 ml/min. Surgical techniques were the same as described previously (Bastian 1996a,b), and all procedures were in accordance with the University of Oklahoma animal care and use guidelines.

Recording

Recordings techniques were the same as used previously (Bastian et al. 2002). Intracellular recordings were made with KCl-filled micropipettes. High-resistance (70- to 150-MΩ) micropipettes were used for receptor afferents, whereas lower-resistance (20–35 MΩ) micropipettes were used for intracellular pyramidal cell recordings. Extracellular single-unit recordings from pyramidal cells were made with metal-filled micropipettes (Frank and Becker 1964). For pyramidal cells, recording sites as determined from surface landmarks and recording depths were limited to the lateral and centrolateral ELL segments. Extracellularly recorded spikes were detected with window discriminators and time stamped

(CED 1401-plus hardware and SpikeII software, resolution = 0.1 ms; Cambridge Electronic Design, Cambridge UK). Intracellularly recorded spikes were detected in the same manner and the membrane potential was A-to-D converted at 10 kHz.

Stimulation

The stimulation protocol was previously described in detail (Bastian et al. 2002); $n = 41$ receptor afferents and $n = 54$ pyramidal cells were studied. The stimuli consisted of amplitude modulations (AMs) of an animal's own electric organ discharge (EOD) that were random in nature. Typical contrasts (modulation amplitude to baseline EOD amplitude ratio) were similar to those used in previous studies (Bastian et al. 2002; Chacron et al. 2003, 2005b,c) and ranged between 10 and 20%. The same AM waveform lasting ≥20 s was repeated four times to compare responses to different trials. These random AMs were produced by multiplying an EOD mimic with zero-mean band limited Gaussian white noise with upper cutoff frequency $f_c = 120$ Hz (8^{th}-order Butterworth filter). The EOD mimic consisted of a train of single sinusoids of a duration slightly less than that of a single EOD cycle synchronized to the zero-crossings of the animal's own EOD. The resulting signal was presented to the animal with either global or local geometry via a World Precision Instrument (A395) linear stimulus isolation unit. With global geometry the stimulus was applied via silver-silver chloride electrodes ~15 cm from the animal on each side. The resulting stimulus is relatively homogeneous over both the ipsilateral and contralateral sides to the ELL recorded from. The amplitude of the field was set to 10 mV/cm without the animal in place, and this served as the reference stimulus level (0 dB). The typical global stimulus amplitude used was −26 dB. With local geometry, the stimulus was applied via a small dipole with 3-mm tip spacing positioned typically 2–3 mm lateral to the fish, and the typical local stimulus amplitude used was also −26 dB. To achieve spatial saturation of the receptive field center, two dipoles spaced 0.5 cm apart were placed in the receptive field center as described previously (Chacron et al. 2003).

Analysis

All reported values in the text are given as means ± SD.

Mutual information estimates

All analysis was performed using custom routines in MATLAB (The MathWorks, Natick, MA). The stimulus waveform was resampled at 2 kHz. The spike train was digitized and also resampled at 2 kHz.

We computed the mutual information rate using the direct method (Reinagel and Reid 2000; Strong et al. 1998) for a separate population of $n = 15$ pyramidal cells. This requires a discretization of the stimulus and response probability spaces (Paninski 2003): we divided the spike train into nonoverlapping bins of width $\Delta\tau$. If n action potentials occurred between times $i\Delta\tau$ and $(i + 1)\Delta\tau$, then the value of bin i was set to n. The entropy rate of the response $H(R)$ was estimated from an unrepeated 500-s-long presentation of stimulus S. The entropy rate of the response given the stimulus $H(R/S)$ was estimated from 250 epochs of the same stimulus sample each lasting 2 s. We used Paninski's best upper bound estimators to correct for undersampling bias in the estimates (Paninski 2003), and the mutual information

rate was computed as $I_{\text{direct}}(\Delta\tau) = H(R) - H(R/S)$. I_{direct} depends on $\Delta\tau$ and will increase with decreasing $\Delta\tau$ (Paninski 2003; Passaglia and Troy 2004; Reinagel and Reid 2000). Thus $I_{\text{direct}}(\Delta\tau)$ is an underestimate of the true information rate of the system. To correct for this, we varied $\Delta\tau$ between 2 and 10 ms in increments of 2 ms and linearly extrapolated to $\Delta\tau \rightarrow 0$ (Passaglia and Troy 2004) to obtain an estimate of MI_{direct}.

We also used the indirect method (Rieke et al. 1996) to quantify the amount of information that can be decoded linearly. The four spike trains obtained in response to repeated presentations of the same stimulus waveform S were labeled R_1–R_4. We computed the cross-spectrum $SR_i(f)$ between the stimulus S and spike train R_i, the stimulus power spectrum $SS(f)$, and the power spectrum $RR_i(f)$ of spike train R_i. All these quantities were computed using multitaper estimation techniques with eight Slepian sequences (Jarvis and Mitra 2001). A lower bound on the rate density of information transmission at frequency f can be computed from the stimulus-response (SR) coherence (Borst and Theunissen 1999; Marsat and Pollack 2004; Rieke et al. 1996)

$$I_{\text{lower}}(f) = -\log_2[1 - C_{\text{SR}}(f)]$$

where $C_{\text{SR}}(f)$ is the SR coherence given by (Rieke et al. 1996; Roddey et al. 2000)

$$C_{\text{SR}}(f) = \frac{\left|\frac{1}{4}\sum_{i=1}^{4}\text{SR}_i(f)\right|^2}{\frac{\text{SS}(f)}{4}\sum_{i=1}^{4}\text{RR}_i(f)}$$

The total information rate MI_{lower} is obtained by integrating $I_{\text{lower}}(f)$ between 0 and the stimulus' cutoff frequency f_c. A comparison between MI_{direct} and MI_{lower} gives the relative amount of information that can be decoded linearly with respect to the total amount of information available. We thus computed the fraction of information that can be recovered by linear means as $\Delta I = 100 * MI_{\text{lower}}/MI_{\text{direct}}$.

Performance of linear and nonlinear encoding models

Roddey et al. (2000) have proposed a method for assessing the performance of neural encoding models: the performance of the best linear model can be assessed by the SR coherence. However, nonlinear models can outperform linear ones and the response-response (RR) coherence gives an upper bound on the performance of the optimal nonlinear model. A comparison between the SR coherence and the square root of the RR coherence will thus quantify the performance of the best linear model with respect to the optimum performance theoretically achievable. The RR coherence is given by (Roddey et al. 2000)

$$C_{\mathrm{RR}}(f)=\frac{\left|\frac{1}{6}\sum_{i=1}^{4}\sum_{j<i}\mathrm{RR}_{\mathrm{ij}}(f)\right|^{2}}{\left(\frac{1}{4}\sum_{i=1}^{4}\mathrm{RR}_{i}(f)\right)^{2}}$$

where RR_{ij} is the cross-spectrum between spike trains R_i and R_j. RR and SR coherence curve estimates were obtained from $n = 41$ receptor afferents and $n = 54$ pyramidal cells.

For pyramidal cell intracellular recordings ($n = 10$), we removed the spike waveforms as described previously (Chacron et al. 2003): spikes were removed from the intracellular signal by replacing the spike waveform by the average of the membrane potential values immediately preceding and following the spike waveform. The resulting signal was then low-passed filtered (8^{th}-order Butterworth, 200-Hz cutoff) and resampled at 2 kHz. We computed the SR and RR coherence estimates between the resulting membrane potential and stimulus in the same manner as for digitized spike trains.

Steps in EOD amplitude were also given to evoke compound excitatory postsynaptic potentials (EPSPs) in a separate population of $n = 9$ E-type pyramidal cells from which we also recorded intracellularly. Each step consisted of a 10–20% increase in EOD amplitude that was 4 ms in duration. Steps were delivered via each dipole separately as well as through both dipoles simultaneously to assess EPSP summation. To prevent spiking, the cell was hyperpolarized by intracellular current injection. Typical currents used were −0.4 nA. Compound EPSP shapes were obtained by averaging membrane potential over ≥40 stimulus presentations.

Spike train dejittering

Aldworth et al. (2005) have proposed a dejittering algorithm to eliminate noise due to spike-timing jitter. Their results show that dejittering can significantly improve the spike-triggered average (STA). To test if spike-timing jitter can significantly influence information processing in the electrosensory system, we implemented their algorithm on $n = 41$ receptor afferents and $n = 54$ pyramidal cells. We refer to Aldworth et al. (2005) for the details of the methodology. Briefly, the STA was obtained by taking the stimulus waveform surrounding each spike and then averaging over all spikes as done previously (Chacron et al. 2005c). Each stimulus waveform was then shifted in time by amounts varying between l_{min} and 3 σ_{t}. The notation is the same as the one used by Aldworth et al. (2005). l_{min} is the minimum response latency which one can estimate from the STA. σ_{t} is an estimate of the spike-timing jitter. Previous studies have estimated spike timing jitter of around 1 ms for pyramidal cells (Chacron et al. 2003). We used a range of values between 1 and 5 ms for σ_{t}, and the results were not sensitive to the value used: we thus present results obtained for $\sigma_{\mathrm{t}} = 5$ ms. The optimal shift time t for each segment was obtained by minimizing the distance measure

$$d=\frac{1}{2}\left(x_{\mathrm{T}}C^{-1}x+\frac{t^2}{\sigma_t^2}\right)$$

Here x is the residual between each stimulus segment and the mean stimulus segment from the previous iteration with x_{T} being the transpose of x. C is the covariance matrix of the stimulus ensemble. This procedure can be iterated until convergence. We used the same convergence criterion as Aldworth et al. (2005). The new STA was then computed from the shifted stimulus segments.

Pharmacology

Micropressure ejection techniques (Bastian 1993; Bastian et al. 2004; Chacron et al. 2005c) were used to apply the non-*N*-methyl-D-aspartate (NMDA) glutamate antagonist 1,6-cyano-7-nitroquinoxa-line-2,3-dione (CNQX) to local regions of the ELL molecular layer containing the apical dendrites of a recorded cell. This was attempted separately on $n = 10$ pyramidal cells. Multibarrel pipettes were pulled to a fine tip and broken back to a total tip diameter of ~10 mm. One barrel was filled with a 1 mM solution of disodium CNQX, and a second barrel was filled with 1 mM solution of glutamate. After a well-isolated single-unit extracellular recording was established, the pressure pipette was slowly advanced into an appropriate region of the ELL molecular layer while periodically ejecting “puffs” of glutamate. Typically ejection duration ranged from 50 to 100 ms and ejection pressure was usually 40 psi. As described earlier (Bastian 1993), proximity to the apical dendrite of the recorded cell was indicated by short-latency increases in firing rate following glutamate ejection. Following correct placement, CNQX was delivered as a single dose or series of pulses (e.g., 100-ms puffs at 0.5 Hz for 20 s), and this treatment typically resulted in tonic alterations in pyramidal cell activity lasting ~5 min.

Modeling

We built a model of receptor afferent input synapsing unto the basilar dendrite of an E-type pyramidal cell with feedback input from higher centers. Each of the $n = 10$ receptor afferents is modeled using a leaky integrate-and-fire mechanism with dynamic threshold (Chacron et al. 2000, 2001, 2005c). The voltage v_i and threshold θ_i of receptor afferent i obey the following differential equations over times between action potentials

$$\dot{V}_i=-\frac{V_i}{\tau_v}+\frac{I_i}{\tau_v}$$
$$\theta_j=(\theta_0-\theta_i)/\tau_\theta$$

with I_i given by

$$I_i=[S(t)+A_0]\sin(2\pi f_{\mathrm{EOD}}t)\times\Theta[\sin(2\pi f_{\mathrm{EOD}}t)][1+\sigma\xi_i(t)]$$

Here, f_{eod} is the EOD frequency, $\Theta(.)$ is the Heaviside function [$\Theta(x) = 0$ if $x < 0$ and $\Theta(x) = 1$ otherwise]), and $\xi_i(t)$ is Gaussian white noise with zero mean and unit variance that is

uncorrelated among different receptors. $S(t)$ is the stimulus with SD 0.2 mV which we take to be low-pass filtered Gaussian white noise with the same cutoff (120 Hz) used in the experiments. When $v_i(t) = \theta_i(t)$, v_i is reset to 0, whereas θ_i is incremented by $\Delta\theta$ and an action potential is said to have occurred. Parameter values used were $A_0 = 0.2613$ mV, $\tau_V = 1$ ms, $\tau_\theta = 14.5$ ms, $\theta_0 = 0.03$, $\Delta\theta = 0.05$, $\sigma = 0.2$, $f_{\mathrm{EOD}} = 700$ Hz. Receptor afferents synapse unto the basilar dendrite of an E-type pyramidal cell, the voltage in the basilar dendrite is given by

$$C\frac{\mathrm{d}V_\mathrm{d}}{\mathrm{d}t} = -g_\mathrm{leak}(V - E_\mathrm{leak}) - g_\mathrm{max}(V - E_\mathrm{rev})\sum_{i=1}^{10}\sum_{j=1}^{\mathrm{M}_j(\mathrm{t})}\frac{t_{ij}}{\tau}\exp\left(-\frac{t_{ij}}{\tau}\right)$$

where $M_i(t)$ is the spike count of afferent i at time t. Previous studies using compartmental models have shown that the long basilar dendrite of superficial E-cells acts as a low-pass filter (Chacron et al. 2005c). Here we implement this in a simple fashion

$$\frac{\mathrm{d}V_s}{\mathrm{d}t} = -\frac{(V_s - V_d)}{\tau_d}$$

where V_s is the membrane potential at the soma. Synaptic noise sources are modeled using an Ornstein-Uhlenbeck process (Gardiner 1985; Manwani and Koch 1999)

$$\frac{\mathrm{d}\lambda}{\mathrm{d}t} = -\frac{\lambda}{\tau_\lambda} + \sqrt{D}\xi(t)$$

where $\xi(t)$ is Gaussian white noise with mean zero and variance unity. λ is added to the somatic membrane potential V_s. $V_s(t) + \lambda(t)$ and $S(t)$ were both sampled at 2 kHz, and we computed upper and lower bounds on the mutual information rate between $S(t)$ and $V_s(t) + \lambda(t)$ in the same manner as for the experimental data. As before (Chacron et al. 2005c), a negative image was created by low-pass filtering a delayed stimulus $S(t - \tau_\mathrm{delay})$ (4^th-order Butterworth, 20-Hz cutoff frequency). τ_delay accounts for conduction times to and from higher centers. The negative image was then multiplied by a gain G_neg and subtracted from V_s. The negative image mimics feedback input that reduces the low-frequency response of pyramidal cells to global stimuli (Bastian 1996a; Bastian et al. 2004; Chacron et al. 2003, 2005c). To mimic local and global geometry, we varied the number of afferents being stimulated N_stim, varied the synaptic noise intensity D, and added the negative image (i.e., $G_\mathrm{neg} > 0$). Table 1 summarizes the parameter values used during simulations.

RESULTS

Good performance for linear encoding models of receptor afferent activity

We first assessed the performance of optimal linear encoding models of receptor afferent activity by comparing the SR coherence to the square rooted RR coherence. Both measures range between 0 and 1. The SR coherence is a measure of linear correlations between the

stimulus S and the response R and quantifies the performance of the optimal linear encoding model (Roddey et al. 2000). On the other hand, the RR coherence is obtained from different responses of the same neuron to repeated presentations of the same stimulus. As such, it is a measure of the trial-to-trial variability of the neural response that cannot be accounted by the stimulus and an upper bound on the performance of any encoding model is given by the square rooted RR coherence (Roddey et al. 2000). A comparison between the SR and square rooted RR coherence curves thus allows us to quantify the performance of optimal linear encoding models with respect to the maximum theoretically achievable performance. Population averaged ($n = 41$) square rooted RR and SR coherence curves for electroreceptor afferents were broadband to weakly low-pass (Fig. 1). We computed the performance index PI of optimal linear encoding models by averaging $100*C_{rs}(f)/[C_{rr}(f)]^{0.5}$ over f between 0 and 120 Hz. For receptor afferents, we obtained PI = 86.27 ± 7.48% (all numerical values obtained experimentally in the text and in tables are given as means ± SD), indicating an overall good performance for linear encoding models. Although conventional tuning curves predict a high-pass tuning for receptor afferents (Bastian 1981; Chacron et al. 2005b; Nelson et al. 1997) due to their strong adaptation (Benda et al. 2005), previous studies have found that lower bound information tuning curves were broadband (Chacron et al. 2005b,c; Wessel et al. 1996) because receptor afferents display low amounts of noise at low frequencies due to intrinsic dynamics (Chacron et al. 2005b). These dynamics manifest themselves by intrinsic negative interspike interval correlations (Chacron et al. 2000, 2001, 2004, 2005b). We conclude that despite strong intrinsic dynamics, linear encoding models are adequate for receptor afferents.

Optimal linear encoding models of pyramidal cell activity perform better under local stimulation than under global stimulation

Unlike receptor afferents, pyramidal cells show sensitivity to the spatial extent of the stimulus (Bastian et al. 2002, 2004; Chacron et al. 2003, 2005c; Doiron et al. 2003). We thus compared the performance of optimal linear encoding models under both local (spatially localized) and global (spatially diffuse) stimulation. As described previously (Chacron et al. 2003, 2005c), E-cells switch their preferred tuning from low to higher temporal frequencies in response to a switch from local to global stimulation geometry (Fig. 2, *A* and *B*), and this switch is seen in both the SR and the square rooted RR coherence curves. We computed the performance index PI as before and obtained $PI_{local} = 48.63 \pm 13.87\%$ for local stimulation and $PI_{global} = 36.80 \pm 13.97\%$ for global stimulation ($P < 10^{-3}$, pairwise t-test, $n = 27$). Overall, linear encoding models thus performed better under local stimulation than under global stimulation.

I cells showed a decrease in low-frequency responsiveness on transitioning from local to global geometry (Fig. 2, *C* and *D*). We obtained $PI_{local} = 38.59 \pm 9.68\%$ and $PI_{global} = 20.82 \pm 7.75\%$ for local and global stimulation geometries, respectively ($P < 10^{-3}$, pairwise t-test, $n = 27$). Similarly to E cells, optimal linear encoding models performed better under local stimulation than global stimulation. Overall, linear encoding models performed significantly better for E cells than for I cells for both local ($P = 0.01$, t-test, $n = 27$) and global stimulation ($P < 10^{-3}$, t-test, $n = 27$). The performance index PI was at most 50% and this

indicates that nonlinear encoding mechanisms are significant in pyramidal cells. Models of their activity must thus take these into account.

Linear decoder performs better under local stimulation than under global stimulation

Information encoded in a nonlinear fashion can sometimes be decoded linearly (Rieke et al. 1996). To gauge the performance of linear decoders, we computed the mutual information rates of pyramidal cells using both the direct and indirect methods. Results obtained under both local and global stimulation are summarized in Table 2. The percentage of information that can be decoded linearly ΔI was higher under local geometry than under global geometry, indicating that at least part of the information nonlinearly encoded by pyramidal cells has to be decoded nonlinearly. We will return to this issue in the discussion but for now we concentrate on understanding the nature of nonlinear encoding mechanisms present in pyramidal cells.

Pyramidal cell dendritic morphology is correlated with nonlinear encoding

We first investigated whether there was any correlation between dendritic morphology and nonlinear encoding. Previous studies have demonstrated a negative correlation between pyramidal cell dendritic morphology and their firing rate (Bastian and Courtright 1991; Bastian and Nguyenkim 2001). We thus plotted PI as a function of firing rate. For local stimuli (Fig. 3*A*), no correlation between the performance index PI of linear encoding models and firing rate was observed ($R = 0.3065$, $P = 0.1199$, $n = 27$). On the other hand, there was a significant positive correlation between PI and firing rate for global stimuli ($R = 0.746$, $P < 10^{-3}$, $n = 27$; Fig. 3*B*). Linear encoding models are thus more apt at describing the behavior of cells with higher firing frequencies and, therefore smaller apical dendrites, under global stimuli. The situation is similar for I cells: we observed a lack of correlation between PI and firing rate for local stimulation ($R = 0.2676$, $P = 0.1771$, $n = 27$; Fig. 3*C*) and a significant correlation under global stimulation ($R = 0.477$, $P = 0.01$, $n = 27$; Fig. 3*D*). These results suggest that dendritic morphology influences linear encoding for both E and I cells with lower PI values for cells that had low firing rates.

Blockade of feedback input can affect the performance of linear encoding models

It is known from previous studies that global stimuli can activate correlated patterns of synaptic input to pyramidal cells in the form of a negative image that cancels low frequency feedforward input (Bastian 1996a,b, 1998; Bastian et al. 2004; Chacron et al. 2005c). This is not the case for local stimulation: previous studies suggest that indirect feedback input to pyramidal cells is uncorrelated with the stimulus for such stimuli (Bastian et al. 2004; Chacron et al. 2005c). As correlated synaptic input into a neuron is known to change its integration properties (Salinas and Sejnowski 2000, 2001), we reversibly blocked indirect feedback input to pyramidal cells to gauge its effects on nonlinear encoding. It is furthermore known from previous studies that the negative image has a similar function in both E- and I-type pyramidal cells (Bastian et al. 2002, 2004; Chacron et al. 2005c). For this reason and because similar changes were seen for both E- and I-type pyramidal cells, the results were pooled.

Pharmacological blockade of feedback input increased the difference between the square rooted RR coherence and the SR coherence under both local (Fig. 4*A*) and global (*B*) stimulation. However, the percent increase was greater under local stimulation, and this is reflected in the performance index PI of optimal linear encoding models. Results are summarized in Table 3. Under local stimulation, blockade of feedback input significantly reduced the performance index of optimal linear models. A small reduction in PI was seen contingent on feedback blockade under global stimulation, but this reduction was not statistically significant.

We now hypothesize as to the possible mechanisms that could explain these results. Under local stimulation, feedback input could act as synaptic noise for pyramidal cells as it is not likely to be correlated with the stimulus (Chacron et al. 2005c). Noise is known to linearize the transfer function of nonlinear systems (Stemmler 1996), and high levels of noise will make a strongly nonlinear system act like a linear one (Chacron et al. 2000, 2005a; Doiron et al. 2004; Lindner et al. 2005). Global stimuli, however, activate feedback input unto pyramidal cells in the form of a negative image of the expected afferent input (Bastian et al. 2004; Chacron et al. 2005c). Feedback input would not be considered as noise in this situation as it would be correlated with the stimulus. There would thus be less noise under global stimulation implying a stronger effect of system nonlinearities thus explaining why linear encoding models perform worse under that geometry. Blocking the negative image under global stimulation would not change the amount of noise (as the feedback pathway would then presumably be silent), and this might explain why feedback blockade did not significantly reduce the performance of linear encoding models under global stimulation.

Receptive field spatial saturation increases nonlinear coding

Local stimuli only impinge on a fraction of the receptive field center of E-type pyramidal cells, whereas global stimuli spatially saturate the receptive field center (Chacron et al. 2003). As such, the fraction of the receptive field center not stimulated might also contribute synaptic noise under local stimulation. Therefore spatially saturating the RF center is expected to reduce synaptic noise and thus presumably worsen the performance of linear encoding models. To test this hypothesis, we spatially saturated the receptive field center of pyramidal cells using a second dipole (see METHODS). The effects of receptive field center spatial saturation are shown in Fig. 5 for E cells. Spatial saturation significantly decreased the performance index PI of linear encoding models ($P = 0.003$, pairwise t-test, $n = 7$; Fig. 5, *A* and *B*). This decreased performance is mostly seen for high frequencies (Fig. 5*B*, *inset*) and is similar to the decreased performance seen as we transition from local to global stimulation geometry. We conclude from this that spatial saturation of the receptive field center will decrease the performance index of optimal linear encoding models.

We hypothesize that this is also due to synaptic noise reduction but from feedforward sources. It is likely that receptive field center saturation does not activate significant feedback input in the form of a negative image (Chacron et al. 2003) and thus would presumably not reduce synaptic noise from feedback sources. The number of spontaneously active receptor afferents uncorrelated with the stimulus, and therefore contributing feedforward synaptic noise will be reduced as receptive field saturation increases. The worse

performance of linear encoding models is again a consequence of reduced synaptic noise from feedforward sources. Previous studies have shown that this synaptic noise should contain more power at high frequencies than at low frequencies (Chacron et al. 2005b). The fact that the performance of optimal linear encoding models was mostly degraded for high frequencies (Fig. 5, *inset*) is consistent with this hypothesis.

The results from this and the previous section have shown the respective contributions of feedforward and -back input in controlling the amount of synaptic noise in pyramidal cells. However, they do not give us the nature of the nonlinear mechanisms by which pyramidal cells encode sensory information.

Nonlinear filtering by pyramidal cell dendrites

Previous studies in the retina have suggested that nonlinear information processing could simply be the result of action potential generation (Passaglia and Troy 2004). Indeed, the firing of single or bursts of action potentials is a very nonlinear phenomenon, and pyramidal cells certainly have the capacity to fire bursts of action potentials both in vitro (Lemon and Turner 2000) and in vivo (Bastian and Nguyenkim 2001). To test whether action potential dynamics were responsible for nonlinear encoding, we recorded intracellularly both from pyramidal cell somata and proximal apical dendrites. We then measured the SR and RR coherence of the membrane potential with spikes removed. It is seen that linear encoding models of the membrane potential performed significantly better under local geometry than global geometry (Fig. 6, *A* and *B*). We had $PI_{local} = 59.86 \pm 19.34\%$ and $PI_{global} = 42.71 \pm 15.82\%$ under local and global stimulation, respectively ($P = 0.002$, pairwise *t*-test, $n = 15$). This change is similar to that seen with pyramidal cell spike trains (compare Figs. 2 and 6).

To ensure that this result was not simply an artifact due to spike removal, we also hyperpolarized pyramidal cells by intracellular current injection. Typical current used to hyperpolarize the cell were −0.4 nA, and this caused a significant reduction in firing frequency that averaged $74.38 \pm 14.1\%$ ($P < 10^{-3}$, pairwise *t*-test, $n = 10$) and furthermore completely eliminated spiking activity in three cells. We compared the relative amount of information that could be decoded linearly from the membrane potential with spikes removed to the one obtained from the membrane potential with spikes removed under hyperpolarization under both local and global stimulation. Results were pooled across local and global stimulation because no difference was seen contingent on stimulation geometry. The membrane potential with spikes removed and the membrane potential with spikes removed under hyperpolarization gave similar PI values that were not significantly different from one another (54.76 ± 19.45 and $53.81 \pm 18.08\%$, respectively, $P = 0.87$, pairwise *t*-test, $n = 10$), and this argues strongly against the hypothesis that the decrease in performance of linear encoding models seen in the membrane potential was an artifact of spike removal.

We conclude that nonlinear filtering by pyramidal cell dendrites is the most likely cause for nonlinear encoding of sensory stimuli. The nonlinear filtering is furthermore most likely not affected by voltage-gated ion channels located close to the soma as these would have been turned off by hyperpolarization. In E cells, nonlinear filtering is probably taking place in both basilar and apical dendrites. I cells, however, have no basilar dendrites and instead

receive receptor afferent input indirectly on their somata by means of inhibitory interneurons that themselves have basilar dendrites (Maler et al. 1981). Nonlinear encoding of sensory information by I cells could originate from nonlinear filtering in the inhibitory interneurons' basilar dendrites as well as from apical dendrites.

EPSP summation in pyramidal cell dendrites

Nonlinear temporal integration of synaptic PSPs can be caused by voltage-dependent amplification due to sodium currents, and such amplification has been demonstrated in a variety of neurons (Andreasen and Lambert 1999; Berman et al. 2001; Crill 1996; Fortune and Rose 2003; Lipowsky et al. 1996; Stuart and Sakmann 1995). Receptive field center saturation, as occurs with global stimulation, would increase synchrony among receptor afferents providing input from the receptive field center of pyramidal cells, thus causing larger fluctuations in the membrane potential as already observed (Chacron et al. 2003). Increased depolarization might thus activate persistent sodium currents leading to nonlinear amplification of EPSPs, which might explain why the performance index of linear encoding models is worse under global stimulation. This is plausible as it has been shown in vitro that pyramidal cells possess persistent sodium currents and that they can amplify synaptic inputs (Berman et al. 1997, 2001; Turner et al. 1994).

Alternatively, the nonlinear filtering could originate from shunting at excitatory synapses located in distal dendrites. Sublinear summation of EPSPs will occur as the membrane potential is driven toward the reversal potential. This shunting would then be present under both local and global stimulation. However, our results suggest that noise in pyramidal cells is significantly greater under local stimulation than global stimulation. This noise might linearize the system (Chacron et al. 2000; Roddey et al. 2000; Stemmler 1996). Global stimuli would decrease both feedforward and -back noise sources revealing the nonlinear effects of shunting. To test which of these two hypotheses is correct, we looked at EPSP summation in pyramidal cells.

We recorded intracellularly from E-type pyramidal cells as they receive direct receptor afferent input on their basilar dendrites (Maler 1979; Maler et al. 1981). Steps in EOD amplitude delivered via one or two dipoles positioned in the cell's receptive field center were used to evoke compound EPSPs. A negative bias current was applied through the recording electrode to maintain the cell below the threshold for action potential generation: note that nonlinear processing is still seen under hyperpolarization. Figure 7 shows the results from one example cell. Compound EPSPs evoked by each dipole separately were similar in shape (Fig. 7*A*). The compound EPSP evoked by both dipoles is larger in magnitude (Fig. 7*B*). However, it is not different from the predicted linear sum of compound EPSPs evoked by each dipole separately. Similar results were seen for eight additional cells. The mean difference between the compound EPSP evoked by both dipoles and the predicted linear sum was not statistically difference from zero ($P = 0.81$, t-test, $n = 9$). Although this result does not rule out the hypothesis that activation of persistent sodium or other voltage-gated conductances are at least partially responsible for increased nonlinear coding of global stimuli, it certainly argues against them being a major source of nonlinear processing in the electrosensory system. We note that linear summation of EPSPs in dendrites is possible

through the interaction of voltage-dependent conductances and has already been observed (Cash and Yuste 1999).

We therefore will concentrate on the second hypothesis: shunting of synaptic EPSPs in distal dendrites as a mechanism for nonlinear encoding of sensory information. To demonstrate the feasibility of such a mechanism, we built a model of receptor afferents converging onto an E cell's basilar dendrite.

Modeling

In this section, we show that shunting at distal excitatory synapses with varying levels of noise is compatible with the experimental results. Using our model, we reproduce the effects of receptive field center saturation, feedback blockade, and finally the effects of transitioning from local to global stimulation.

We first model the effects of receptive field center saturation. Previous results have shown that the negative image is not significantly evoked by either one- or two-dipole stimulation (Bastian et al. 2004; Chacron et al. 2003, 2005c). We thus do not include a negative image in the model at this time (i.e., $G_{neg} = 0$). There is, however, synaptic noise from feedback sources (i.e., $D > 0$) that is not correlated with the stimulus. To mimic local stimulation, only a fraction of receptor afferents converging on the model pyramidal cell received stimulation. Square rooted RR (black) and SR (gray) coherence curves are shown in Fig. 8*A* and closely resembled the curves obtained experimentally under local stimulation (compare with Fig. 2*A*). To mimic receptive field saturation, we increased the percentage of receptor afferents receiving stimulation. Square rooted RR (black) and SR (gray) coherence curves are shown in Fig. 8*B* and resembled the curves obtained under receptive field center saturation (compare Figs. 8*B* and 5*B*). As in the experimental data, there was a significant decrease in the performance of linear encoding models: the *inset* of Fig. 8*B* shows that the performance index PI decreases as a function of the percentage of receptor afferents receiving stimuli. Our modeling results so far thus agree qualitatively with the experimental data on receptive field center saturation.

We now concentrate on the effects of feedback blockade by adding a negative image to the model (i.e., $G_{neg} > 0$). Figure 9*A* shows that adding a negative image does not affect the performance of linear encoding models. This is because the negative image is a linear transformation of the stimulus that is then added to the membrane potential. The *inset* of Fig. 9*A* shows that addition of the negative image reduced the low-frequency response as seen experimentally, and this result also mimics the effects of feedback blockade under global stimulation (compare Figs. 9*A* and 4*B*).

To clarify the influence of feedback synaptic noise on the performance of linear encoding models, we varied the amount of synaptic noise from feedback sources in the model. Figure 9*B* shows the performance index PI of linear encoding models as a function of synaptic noise intensity *D*. PI increases as a function of D. Thus decreasing the amount of feedback synaptic noise "reveals" the presence of the shunting nonlinearity in the model that then causes a decrease in the performance of linear encoding models.

So far our results suggest that transitioning from local to global geometry has two major effects: first, spatial saturation of the receptive field center increases the fraction of receptor afferents being stimulated and thus reduces the amount of feedforward synaptic noise. Second, activation of the negative image reduces the amount of feedback synaptic noise. We thus increased the fraction of receptor afferents being stimulated, added the negative image, and reduced the feedback synaptic noise intensity D in the model. Figure 9C shows the square rooted RR and SR coherence curves obtained with the model under "global" stimulation. A comparison with "local" stimulation (Fig. 8A) shows the same qualitative changes as in the experimental data (compare Figs. 8A and 9C with 2, A and B, respectively). Our modeling results thus show that shunting at excitatory synapses is compatible with the experimental results.

DISCUSSION

Performance of optimal linear encoding models

Although linear encoding models were found to be adequate for receptor afferents, they were in general inadequate for pyramidal cells. In particular, linear encoding models performed better for E cells than for I cells, and this shows that there are significant asymmetries between E and I cells. Previous studies on retinal ganglion cells have shown significant asymmetries between ON and OFF type cells (Chichilnisky and Kalmar 2002), and these asymmetries maybe a general feature of sensory processing. In the electrosensory system, this may be due to the fact that I cells receive receptor afferent input indirectly through inhibitory interneurons (Maler 1979; Maler et al. 1981). Further, I cells have a significantly smaller receptive field center area than E cells (Bastian et al. 2002). Thus local stimulation is expected to stimulate a greater fraction of I-cell receptive field centers than of E-cell receptive field centers, possibly explaining why linear encoding models are less apt at describing I-cell behavior. Further studies are needed to find the neural mechanisms responsible for these asymmetries.

It was seen that linear encoding models were more apt to describe pyramidal cell responses to spatially localized stimuli than spatially diffuse stimuli. Similar results are seen in retinal ganglion cells (Passaglia and Troy 2004). These spatially diffuse stimuli result in an increased effective stimulation of the receptive field center (Chacron et al. 2003) thus increasing the net stimulus intensity. Stimulus intensity has been shown to affect the performance of linear encoding models in both the cricket cercal (Roddey et al. 2000) and auditory (Marsat and Pollack 2004, 2005) systems. Nonlinear encoding models are thus necessary to describe neural responses to strong stimuli, and this may be a general feature of sensory processing.

Our results show that both feedforward and feedback mechanisms can affect the overall level of noise in pyramidal cells. Spatially diffuse stimuli were shown to attenuate feedforward noise sources through receptive field center saturation and attenuated feedback noise sources through activation of the negative image. This implies that the neural code should be different for electrolocation and electrocommunication stimuli. We hypothesize that temporal integration of receptor afferent evoked EPSPs might occur under local stimulation whereas coincidence detection of synchronized input might occur under global stimulation.

The fact that superficial (i.e., low firing rate) pyramidal cells show significantly larger integration time constants as assessed from spike-triggered averages under local stimulation than under global stimulation (Chacron et al. 2005c) supports this hypothesis.

Pyramidal cell heterogeneities were found to influence the performance of linear encoding models. Superficial pyramidal cells with the largest apical dendrites were found to have the greatest change in the performance of nonlinear encoding models by transitioning from local to global stimulation, whereas deep pyramidal cells showed no significant change. We suggest that this may be due to their larger receptive field centers (Bastian et al. 2002) as well as the greater amounts of feedback input that they receive (Bastian et al. 2004). Both would contribute to greater amounts of noise under local stimulation. The high coefficient of variations displayed by superficial pyramidal cells support this hypothesis (Bastian and Nguyenkim 2001).

Validity of previous studies in the electrosensory system

The results presented in this study do not invalidate previous results establishing the tuning of receptor afferents and pyramidal cells as both the SR and RR coherence curves had similar shapes. This is similar to other studies in other systems using broadband noise stimuli (Marsat and Pollack 2004; Roddey et al. 2000). Differences between the SR and RR coherence curves appear when stronger spatially diffuse as well as narrowband stimuli are used (data not shown), and further studies are needed to quantify these effects.

We have shown that previously published mutual information rates using the indirect method severely underestimated the information transmission capabilities of pyramidal cells. However, the similarity between the SR and RR coherence curves show that previously published SR coherence curves were at least qualitatively correct. Some of these previous studies found that pyramidal cells transmitted less information than receptor afferents and were more adept at detecting features of the stimulus (Gabbiani et al. 1996; Metzner et al. 1998). Our results show that this is certainly true for superficial pyramidal cells. However, deep pyramidal cells are in general broadly tuned (Chacron et al. 2005b,c), and our results confirm earlier ones. In particular, deep E-type pyramidal cells were most similar to receptor afferents in their tuning. Thus while superficial pyramidal cells are highly selective in their responses, deep pyramidal cells are not selective and instead encode every aspect of the noise stimulus. In fact, the information from the deep pyramidal cells is used to increase the selectivity of superficial pyramidal cells under global stimulation via a feedback mechanism (Bastian et al. 2004).

Nature of nonlinear encoding by pyramidal cells

A novel aspect of this study was the investigation of the nature of nonlinear encoding by pyramidal cells. Intracellular recordings showed that nonlinear encoding could be decomposed into two parts: a nonlinear filtering of the stimulus by distal dendrites followed by a mostly linear encoding of the resulting neural signal by the spiking mechanism. Because the passive cable equation is linear, it cannot account for the nonlinear processing seen in ELL pyramidal cells. Thus either voltage-dependent conductances or synaptic processes such as sodium currents (Andreasen and Lambert 1999; Berman et al. 2001; Crill

1996; Lipowsky et al. 1996; Stuart and Sakmann 1995), potassium currents (Cash and Yuste 1999; Magee 1999; Urban and Barrionuevo 1998), shunting inhibition (Ariel and Kogo 2005; Borg-Graham et al. 1998; Higley and Contreras 2003), or shunting excitation (Kogo and Ariel 1999) had to account for nonlinear filtering in dendrites.

Experiments and modeling suggest that the nature of the nonlinear filtering by distal dendrites is shunting at excitatory synapses because compound EPSP summation is mostly linear. This shunting could occur in the basilar bushes of E cells and inhibitory interneurons providing input to I cells as well as the distal apical dendrites of both E and I-cells that receive feedback input. Our modeling suggests that shunting would occur in the basilar bush at the synapse for E-type pyramidal cells, whereas EPSP summation would occur at branch points in the basilar bush. Thus shunting would not in principle preclude linear EPSP summation as we observe. Linear EPSP summation could be made possible by voltage-gated channels (Cash and Yuste 1999), and further experiments carried out in vitro are necessary to verify this. Shunting might cause information loss due to synaptic saturation. However, this loss would occur for very strong stimuli and may thus not impinge on the animal's behavioral abilities. Further, shunting would have the advantage of keeping a neuron within its dynamic range and thus not compromise the detection of weaker stimuli.

We note that our results do not completely exclude the possibility of nonlinear integration of synaptic PSPs via voltage-gated sodium channels. Such nonlinear summation has been shown for pyramidal cells in vitro and was mediated by persistent sodium channels (Berman et al. 2001), and these might contribute to nonlinear filtering. Finally, other processes such as gain control (Bastian 1986) and adaptation (Bastian and Courtright 1991) could also contribute to nonlinear encoding of sensory stimuli by pyramidal cells.

Decoding of information transmitted by pyramidal cell spike trains

Our results show that information encoded nonlinearly by pyramidal cells has to at least in part be decoded in a nonlinear manner: a linear decoder only has access to a fraction of the information transmitted by pyramidal cells. This fraction was greatest for spatially localized stimuli and decreased for spatially diffuse stimuli and our results are similar to those obtained in other systems (Passaglia and Troy 2004). We note that an upper bound on the rate of information transmission can be obtained from the RR coherence curve (Passaglia and Troy 2004; Marsat and Pollack 2004,2005). However, this upper bound can overestimate the amount of information transmitted by a significant amount (Passaglia and Troy 2004), and comparisons obtained using this estimate might underestimate the relative amount of information available to a linear decoder. Our results were obtained by comparing the lower bound obtained by the indirect method to the information rate estimated using the direct method and thus give us a more realistic estimate of the relative amount of information available to a linear decoder.

Previous studies of the electrosensory system almost exclusively used linear decoding algorithms to establish the tuning of receptor afferents and pyramidal cells to various stimuli (Bastian et al. 2002; Chacron et al. 2003, 2005b,c; Gabbiani et al. 1996; Krahe et al. 2002; Kreiman et al. 2000; Metzner et al. 1998; Wessel et al. 1996). Metzner et al. (1998) have considered a particular nonlinear decoder, a second-order Wiener-Volterra Kernel expansion,

and found little improvement as a compared with a linear decoder. In contrast, we used the direct method which makes no assumptions on the nature of the neural code (Reinagel and Reid 2000; Strong et al. 1998) and found that as much as 60% of the information transmitted by pyramidal cells could not be accessed by a linear decoder. This suggests that higher-order neurons should perform nonlinear operations on incoming pyramidal cell spike trains to access this information. Previous studies of Toral neurons receiving input from pyramidal cells have shown nonlinear filtering of sensory input in the form of nonlinear PSP summation via voltage-gated sodium currents (Fortune and Rose 2003) as well as short-term synaptic depression (Fortune and Rose 1997). Recordings from Toral neurons using stimuli similar to those used here are necessary to compare their performance to optimal linear and nonlinear decoders.

Conclusion

To conclude, we have shown nonlinear encoding of sensory information by pyramidal cells. We have investigated the dependence of this on stimulus intensity by varying the spatial extent and found results similar to those obtained in the visual (Passaglia and Troy 2004), auditory (Marsat and Pollack 2004, 2005) and cercal (Roddey et al. 2000) systems. The mechanisms described here will thus most likely share some commonality with other sensory systems. For example, the nonlinear coding in retinal ganglion cells (Passaglia and Troy 2004) could be due to nonlinear integration of photoreceptor input. Such nonlinear integration has been shown in both modeling (Hennig et al. 2002) and experimental (Lee et al. 1989) studies, and it will be interesting to compare nonlinear encoding and decoding mechanisms across sensory systems.

Acknowledgments

The author thanks Dr. Joseph Bastian for help and encouragement with experimental techniques as well as useful discussions and Dr. Leonard Maler for useful discussions.

GRANTS

This research was supported by a postdoctoral fellowship from the Canadian Institutes of Health Research and by the National Institutes of Health.

References

Aldworth ZN, Miller JP, Gedeon T, Cummings GJ, Dimitrov AG. Dejittered spike-conditioned Stimulus waveforms yield improved estimates of neuronal feature selectivity and spike-timing precision of sensory interneurons. J Neurosci. 2005; 25:5323–5332. [PubMed: 15930380]

Andreasen M, Lambert JDC. Somatic amplification of distally generated subthreshold EPSPs in rat hippocampal pyramidal neurons. J Physiol. 1999; 519:85–100. [PubMed: 10432341]

Ariel M, Kogo N. Shunting Inhibition in accessory optic system neurons. J Neurophysiol. 2005; 93:1959–1969. [PubMed: 15563556]

Bastian J. Electrolocation. I. How the electroreceptors of *Apteronotus albifrons* code for moving objects and other electrical stimuli. J Comp Physiol [A]. 1981; 144:465–479.

Bastian J. The role of amino acid neurotransmitters in the descending control of electroreception. J Comp Physiol A. 1993; 172:409–423. [PubMed: 7686228]

Bastian J. Gain control in the electrosensory system mediated by descending inputs to the electrosensory lateral line lobe. J Neurosci. 1986; 6:553–562. [PubMed: 3950710]

Bastian J. Plasticity in an electrosensory system. I. General features of a dynamic sensory filter. J Neurophysiol. 1996a; 76:2483–2496. [PubMed: 8899621]

Bastian J. Plasticity in an electrosensory system. II. Postsynaptic events associated with a dynamic sensory filter. J Neurophysiol. 1996b; 76:2497–2507. [PubMed: 8899622]

Bastian J. Plasticity in an electrosensory system. III. Contrasting properties of spatially segregated dendritic inputs. J Neurophysiol. 1998; 79:1839–1857. [PubMed: 9535952]

Bastian J, Chacron MJ, Maler L. Receptive field organization determines pyramidal cell stimulus-encoding capability and spatial stimulus selectivity. J Neurosci. 2002; 22:4577–4590. [PubMed: 12040065]

Bastian J, Chacron MJ, Maler L. Plastic and non-plastic cells perform unique roles in a network capable of adaptive redundancy reduction. Neuron. 2004; 41:767–779. [PubMed: 15003176]

Bastian J, Courtright J. Morphological correlates of pyramidal cell adaptation rate in the electrosensory lateral line lobe of weakly electric fish. J Comp Physiol [A]. 1991; 168:393–407.

Bastian J, Nguyenkim J. Dendritic modulation of burst-like firing in sensory neurons. J Neurophysiol. 2001; 85:10–22. [PubMed: 11152701]

Benda J, Longtin A, Maler L. Spike-frequency adaptation separates transient communication signals from background oscillations. J Neurosci. 2005; 25:2312–2321. [PubMed: 15745957]

Berman N, Dunn RJ, Maler L. Function of NMDA receptors and persistent sodium channels in a feedback pathway of the electrosensory system. J Neurophysiol. 2001; 86:1612–1621. [PubMed: 11600624]

Berman NJ, Plant J, Turner R, Maler L. Excitatory amino acid transmission at a feedback pathway in the electrosensory system. J Neurophysiol. 1997; 78:1869–1881. [PubMed: 9325356]

Borg-Graham LJ, Monier C, Fregnac Y. VIsual Input evokes transient and strong shunting inhibition in visual cortical neurons. Nature. 1998; 393:369–373. [PubMed: 9620800]

Borst A, Theunissen F. Information theory and neural coding. Nat Neurosci. 1999; 2:947–957. [PubMed: 10526332]

Cash S, Yuste R. Linear summation of excitatory inputs by CA1 pyramidal neurons. Neuron. 1999; 22:383–394. [PubMed: 10069343]

Chacron MJ, Doiron B, Maler L, Longtin A, Bastian J. Non-classical receptive field mediates switch in a sensory neuron's frequency tuning. Nature. 2003; 423:77–81. [PubMed: 12721628]

Chacron MJ, Lindner B, Longtin A. Noise shaping by interval correlations increases information transfer. Phys Rev Lett. 2004; 92:080601. [PubMed: 14995762]

Chacron MJ, Longtin A, Maler L. Delayed excitatory and inhibitory feedback shape neural information transmission. Phys Rev E. 2005a; 72:051917.

Chacron MJ, Longtin A, Maler L. Negative interspike interval correlations increase the neuronal capacity for encoding time-varying stimuli. J Neurosci. 2001; 21:5328–5343. [PubMed: 11438609]

Chacron MJ, Longtin A, St-Hilaire M, Maler L. Suprathreshold stochastic firing dynamics with memory in P-type electroreceptors. Phys Rev Lett. 2000; 85:1576–1579. [PubMed: 10970558]

Chacron MJ, Maler L, Bastian J. Electroreceptor neuron dynamics shape information transmission. Nat Neurosci. 2005b; 8:673–678. [PubMed: 15806098]

Chacron MJ, Maler L, Bastian J. Feedback and feedforward control of frequency tuning to naturalistic stimuli. J Neurosci. 2005c; 25:5521–5532. [PubMed: 15944380]

Chichilnisky EJ, Kalmar RS. Functional asymmetries in ON and OFF ganglion cells of primate retina. J Neurosci. 2002; 22:2737–2747. [PubMed: 11923439]

Cover, T., Thomas, J. Elements of Information Theory. New York: Wiley; 1991.

Crill WE. Persistent sodium current in mammalian central neurons. Annu Rev Physiol. 1996; 58:349–362. [PubMed: 8815799]

De Ruyter van Steveninck RR, Lewen GD, Strong SP, Koberle R, Bialek W. Reproducibility and variability in neural spike trains. Science. 1997; 275:1805–1808. [PubMed: 9065407]

Doiron B, Chacron MJ, Maler L, Longtin A, Bastian J. Inhibitory feedback required for network oscillatory responses to communication but not prey stimuli. Nature. 2003; 421:539–543. [PubMed: 12556894]

Doiron B, Lindner B, Longtin A, Maler L, Bastian J. Oscillatory activity in electrosensory neurons increases with the spatial correlation of the stochastic input stimulus. Phys Rev Lett. 2004; 93:048101. [PubMed: 15323795]

Fortune ES, Rose G. Passive and active membrane properties contribute to the temporal filtering properties of midbrain neurons in vivo. J Neurosci. 1997; 17:3815–3825. [PubMed: 9133400]

Fortune ES, Rose GJ. Voltage-gated Na^+ channels enhance the temporal filtering properties of electrosensory neurons in the torus. J Neurophysiol. 2003; 90:924–929. [PubMed: 12750421]

Frank, K., Becker, MC. Physical Techniques in Biological Research. New York: Academic; 1964. Microelectrodes for recording and stimulation; p. 23-84.

Gabbiani F. Coding of time varying signals in spike trains of linear and half-wave rectifying neurons. Network. 1996; 7:61–85.

Gabbiani F, Metzner W, Wessel R, Koch C. From stimulus encoding to feature extraction in weakly electric fish. Nature. 1996; 384:564–567. [PubMed: 8955269]

Gardiner, CW. Handbook of Stochastic Methods. Berlin: Springer; 1985.

Hennig MH, Funke K, Worgotter F. The Influence of different retinal subcircuits on the nonlinearity of ganglion cell behavior. J Neurosci. 2002; 22:8726–8738. [PubMed: 12351748]

Higley MJ, Contreras D. Nonlinear integration of sensory responses in the rat barrel cortex: an intracellular study in vivo. J Neurosci. 2003; 23:10190–10200. [PubMed: 14614077]

Jarvis MR, Mitra PP. Sampling properties of the spectrum and coherency of sequences of action potentials. Neural Comp. 2001; 13:717–749.

Kogo N, Ariel M. Response attenuation during coincident afferent excitatory inputs. J Neurophysiol. 1999; 81:2945–2955. [PubMed: 10368411]

Krahe R, Gabbiani F. Burst firing in sensory systems. Nat Rev Neurosci. 2004; 5:13–23. [PubMed: 14661065]

Krahe R, Kreiman G, Gabbiani F, Koch C, Metzner W. Stimulus encoding and feature extraction by multiple sensory neurons. J Neurosci. 2002; 22:2374–2382. [PubMed: 11896176]

Kreiman G, Krahe R, Metzner W, Koch C, Gabbiani F. Robustness and variability of neuronal coding by amplitude sensitive afferents in the weakly electric fish eigenmania. J Neurophysiol. 2000; 84:189–224. [PubMed: 10899196]

Lee BB, Martin PR, Valberg A. Nonlinear summation of M- and L-cone inputs to phasic retinal ganglion cells of the macaque. J Neurosci. 1989; 9:1433–1442. [PubMed: 2703886]

Lemon N, Turner RW. Conditional backpropagation generates burst discharge in a sensory neuron. J Neurophysiol. 2000; 89:1519–1530.

Lindner B, Chacron MJ, Longtin A. Integrate-and-fire neurons with threshold noise: a tractable model of how interspike interval correlations affect neuronal signal transmission. Phys Rev E. 2005; 72:021911.

Lipowsky R, Gillessen T, Alzheimer C. Dendritic Na^+ channels amplify EPSPs in hippocampal CA1 pyramidal cells. J Neurophysiol. 1996; 76:2181–2191. [PubMed: 8899593]

Magee JC. Dendritic I_h normalizes hippocampal temporal summation in hippocampal CA1 neurons. Nat Neurosci. 1999; 2:508–514. [PubMed: 10448214]

Mainen ZF, Sejnowski TJ. Reliability of spike timing in neocortical neurons. Science. 1995; 268:1503–1506. [PubMed: 7770778]

Maler L. The posterior lateral line lobe of certain gymnotiform fish. Quantitative light microscopy. J Comp Neurol. 1979; 183:323–363. [PubMed: 762262]

Maler L, Sas EK, Rogers J. The cytology of the posterior lateral line lobe of high frequency weakly electric fish (*Gymnotoidei*): differentiation and synaptic specificity in a simple cortex. J Comp Neurol. 1981; 195:87–139. [PubMed: 7204653]

Manwani A, Koch C. Detecting and estimating signals in noisy cable structure. I. Neuronal noise sources. Neural Comp. 1999; 11:1797–1829.

Marsat G, Pollack GS. Differential temporal coding of rhythmically diverse acoustic signals by a single interneuron. J Neurophysiol. 2004; 92:939–948. [PubMed: 15044517]

Marsat G, Pollack GS. Effect of the temporal pattern of contralateral inhibition on sound localization cues. J Neurosci. 2005; 25:6137–6144. [PubMed: 15987943]

Metzner W, Koch C, Wessel R, Gabbiani F. Feature extraction by burst-like spike patterns in multiple sensory maps. J Neurosci. 1998; 18:2283–2300. [PubMed: 9482813]

Nelson ME, MacIver MA. Prey capture in the weakly electric fish *Apteronotus leptorhynchus*: sensory acquisition strategies and electrosensory consequences. J Exp Biol. 1999; 202:1195–1203. [PubMed: 10210661]

Nelson ME, Xu Z, Payne JR. Characterization and modeling of P-type electrosensory afferent responses to amplitude modulations in a wave-type electric fish. J Comp Physiol [A]. 1997; 181:532–544.

Paninski L. Estimation of entropy and mutual information. Neural Comp. 2003; 15:1191–1253.

Passaglia CL, Troy JB. Information transmission rates of cat retinal ganglion cells. J Neurophysiol. 2004; 91:1217–1229. [PubMed: 14602836]

Reinagel P, Reid RC. Temporal coding of visual information in the thalamus. J Neurosci. 2000; 20:5392–5400. [PubMed: 10884324]

Rieke, F. Physical Principles Underlying Sensory Processing and Computation. Berkeley, CA: University of California; 1992.

Rieke, F., Warland, D., de Ruyter van Steveninck, RR., Bialek, W. Spikes: Exploring the Neural Code. Cambridge, MA: MIT; 1996.

Roddey JC, Girish B, Miller JP. Assessing the performance of neural encoding models in the presence of noise. J Comp Neurosci. 2000; 8:95–112.

Salinas E, Sejnowski TJ. Impact of correlated synaptic input on output firing rates and variability in simple neuronal models. J Neurosci. 2000; 20:6193–6209. [PubMed: 10934269]

Salinas E, Sejnowski TJ. Correlated neuronal activity and the flow of neural information. Nat Rev Neurosci. 2001; 2:539–550. [PubMed: 11483997]

Saunders J, Bastian J. The physiology and morphology of two classes of electrosensory neurons in the weakly electric fish *Apteronotus Leptorhynchus*. J Comp Physiol [A]. 1984; 154:199–209.

Shannon CE. The mathematical theory of communication. Bell Syst Tech J. 1948; 27379–423:623–656.

Stemmler M. A single spike suffices: the simplest form of stochastic resonance in model neurons. Network. 1996; 7:687–716.

Strong SP, Koberle R, de Ruyter van Steveninck RR, Bialek W. Entropy and information in neural spike trains. Phys Rev Lett. 1998; 80:197–200.

Stuart G, Sakmann B. Amplification of EPSPs by axosomatic sodium channels in neocortical pyramidal neurons. Neuron. 1995; 15:1065–1076. [PubMed: 7576650]

Theunissen F, Roddey JC, Stufflebeam S, Clague H, Miller JP. Information theoretic analysis of dynamical encoding by four identified interneurons in the cricket cercal system. J Neurophysiol. 1996; 75:1345–1364. [PubMed: 8727382]

Treves A. On the perceptual structure of face space. Biosystems. 1997; 40:189–196. [PubMed: 8971211]

Turner RW, Maler L, Burrows M. Electroreception and electrocommunication. J Exp Biol. 1999; 202:1167–1458. [PubMed: 10210659]

Turner RW, Maler L, Deerinck T, Levinson SR, Ellisman MH. TTX-sensitive dendritic sodium channels underlie oscillatory discharge in a vertebrate sensory neuron. J Neurosci. 1994; 14:6453–6471. [PubMed: 7965050]

Urban NN, Barrionuevo G. Active summation of excitatory postsynaptic potentials in hippocampal CA3 pyramidal neurons. Proc Natl Acad Sci USA. 1998; 95:11450–11455. [PubMed: 9736757]

Wessel R, Koch C, Gabbiani F. Coding of time-varying electric field amplitude modulations in a wave-type electric fish. J Neurophysiol. 1996; 75:2280–2293. [PubMed: 8793741]

Zupanc GKH, Maler L. Evoked chirping in the weakly electric fish *Apteronotus leptorhynchus*: a quantitative biophysical analysis. Can J Zoo. 1993; 71:2301–2310.

APPENDIX A: EFFECTS OF SPIKE TIMING JITTER

We note that recent results have shown that the spike-triggered average (STA) used for computing the SR coherence underestimated the feature selectivity of cricket interneurons (Aldworth et al. 2005). Therefore the SR coherence and the lower bound on the mutual information rate derived from it could potentially underestimate the information rate of the system due to spike timing jitter. We tested for the effects of spike timing jitter on receptor afferents and found negligible effects on the STA (Fig. A1). This is consistent with previous results showing that spike timing jitter had negligible effects on information transmission by receptor afferents (Kreiman et al. 2000). Furthermore, spike timing jitter in pyramidal cells is on the order of 1 ms (Chacron et al. 2003), which is much less than the correlation time of the stimuli used in this study: 8.33 ms. Thus spike timing jitter is not expected to have much of an effect (Aldworth et al. 2005), and Fig. A2 shows that this is indeed the case. Thus spike timing jitter does not seem to play a role for the stimuli used in this study. The lower bound on the information rate obtained from the SR coherence underestimates the information rate of the system estimated from the direct method and this is due to system nonlinearities other than spike timing jitter.

APPENDIX B: COMPARISON BETWEEN THE UPPER BOUND AND THE DIRECT METHOD

We note that the RR coherence can be used to compute an upper bound MI_{upper} on the mutual information rate (Marsat and Pollack 2004, 2005; Passaglia and Troy 2004). This upper bound may overestimate the information rate as estimated from the direct method (Passaglia and Troy 2004). Table 4 shows population averaged values obtained under local and global geometry. Although there was no significant difference seen under local geometry, the upper bound method can significantly overestimate the mutual information rate as estimated from the direct method. This is similar to what is seen in other systems (Passaglia and Troy 2004).

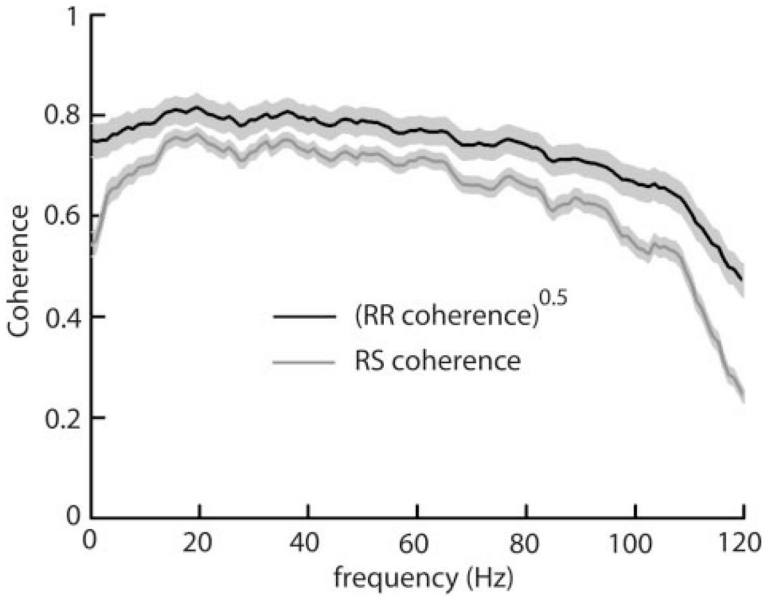

FIG. 1.

Population averaged ($n = 41$) square rooted RR coherence (black) and SR coherence (gray) curves for receptor afferents under global stimulation. On a scale ranging between 0 and 1, the SR coherence quantifies the performance of linear encoding models while the square rooted RR coherence measures the variability that cannot be accounted for by the stimulus and thus gives an upper bound on the SR coherence (see text for explanation). Both curves are qualitatively similar in shape showing a weakly low-pass response. Light gray bands show ± 1 SE.

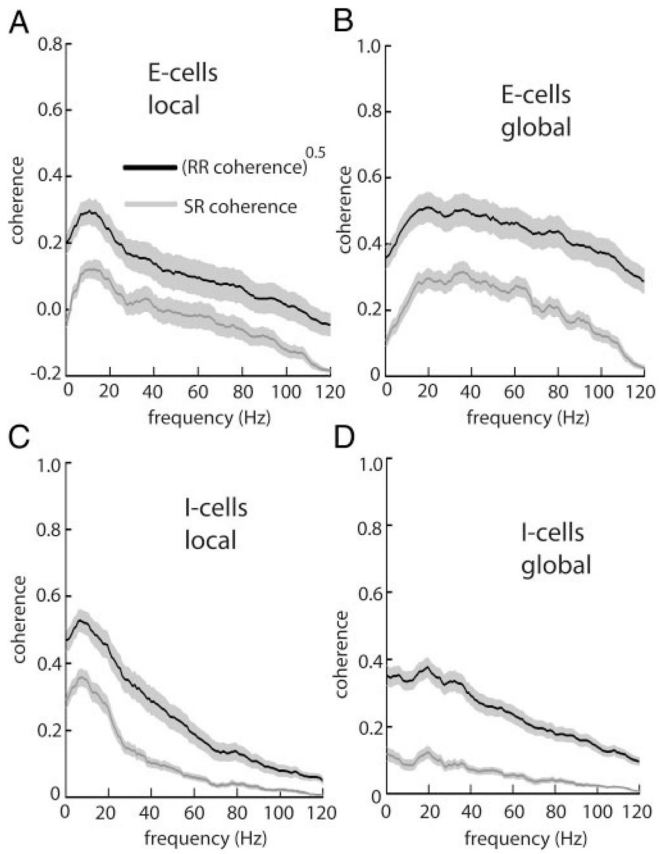

FIG. 2.

A: population averaged ($n = 27$) square rooted RR coherence (black) and SR coherence (gray) for E-type pyramidal cells under local stimulation. *B*: same quantities under global stimulation. *C*: population averaged ($n = 27$) square rooted RR coherence (black) and SR coherence (gray) for I-type pyramidal cells under local stimulation geometry. *D*: same quantities under global stimulation. Light gray bands show ±1 SE.

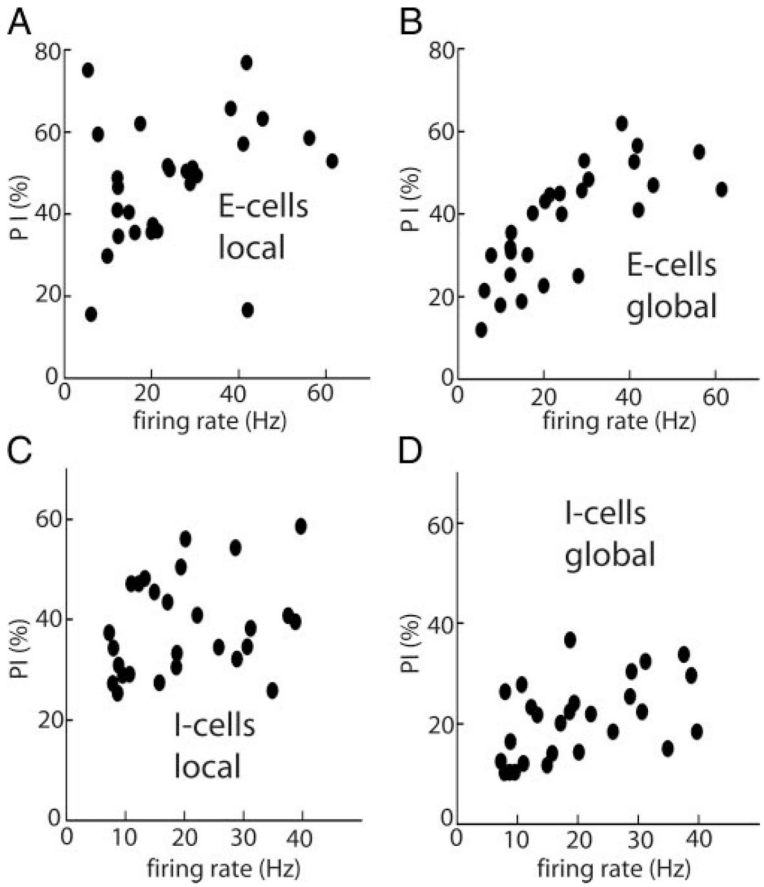

FIG. 3.

A: performance index PI of optimal linear encoding models as a function of cell firing rate for E cells under local stimulation. *B*: same under global stimulation. *C*: performance index PI of optimal linear encoding models as a function of cell firing rate for I cells under local stimulation. *D*: same under global stimulation.

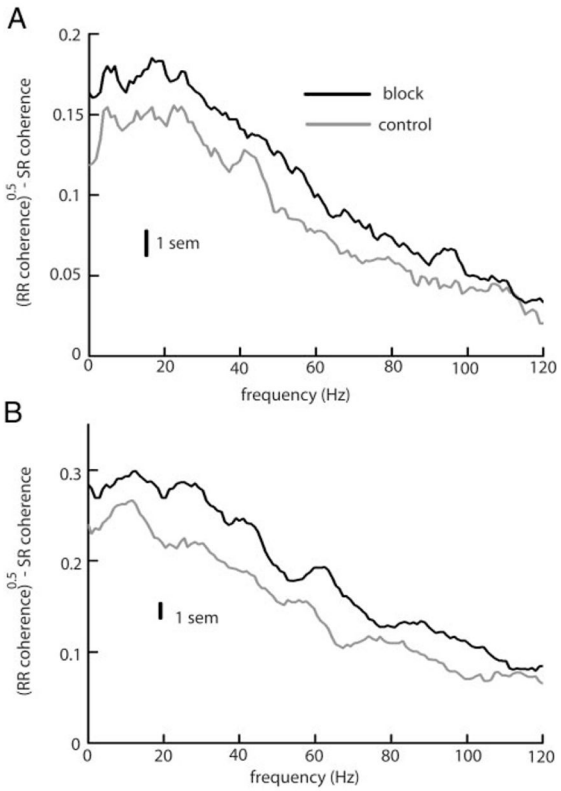

FIG. 4.

A: population averaged ($n = 10$) differences between the square rooted RR coherence and the SR coherence under control (gray) and block (black) for local stimulation. *B*: population averaged ($n = 10$) differences between the square rooted coherence and the SR coherence under control (gray) and block (black) for global stimulation. Vertical bars indicate the SE measured at 10 Hz.

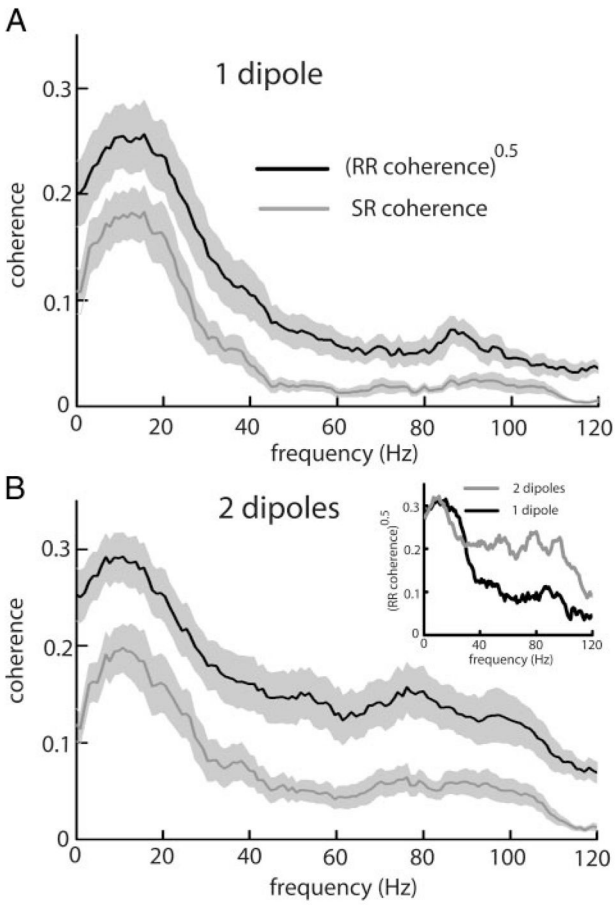

FIG. 5.

A: population averaged ($n = 7$) square rooted RR coherence (black) and SR coherence (gray) for E-type pyramidal cells under 1-dipole (local) stimulation. *B*: same quantities under 2-dipole stimulation. *Inset*: the square rooted RR coherence of an example pyramidal cell under local (black) and 2-dipole (gray) stimulation. Light gray bands show ±1 SE.

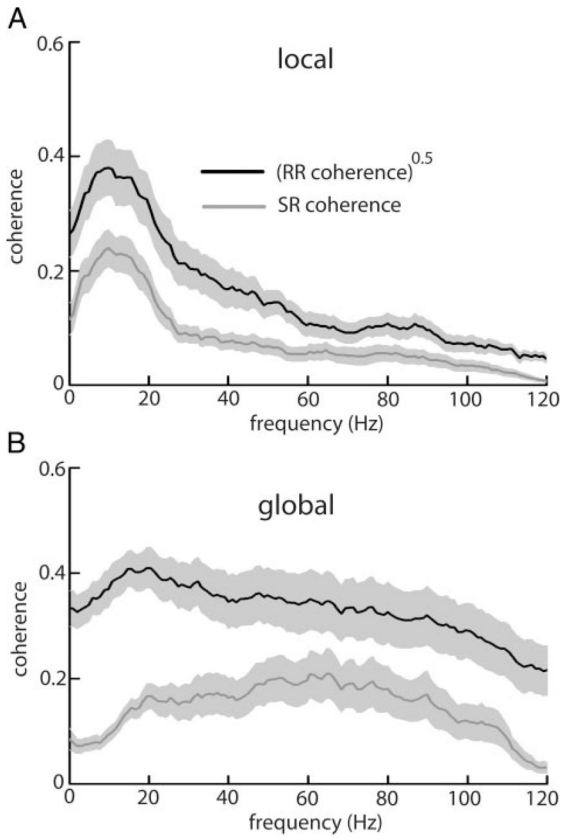

FIG. 6.

A: population averaged ($n = 15$) square rooted RR coherence (black) and SR coherence (gray) computed from the membrane potential under local stimulation geometry. *B*: same quantities under global stimulation. Light gray bands show ±1 SE.

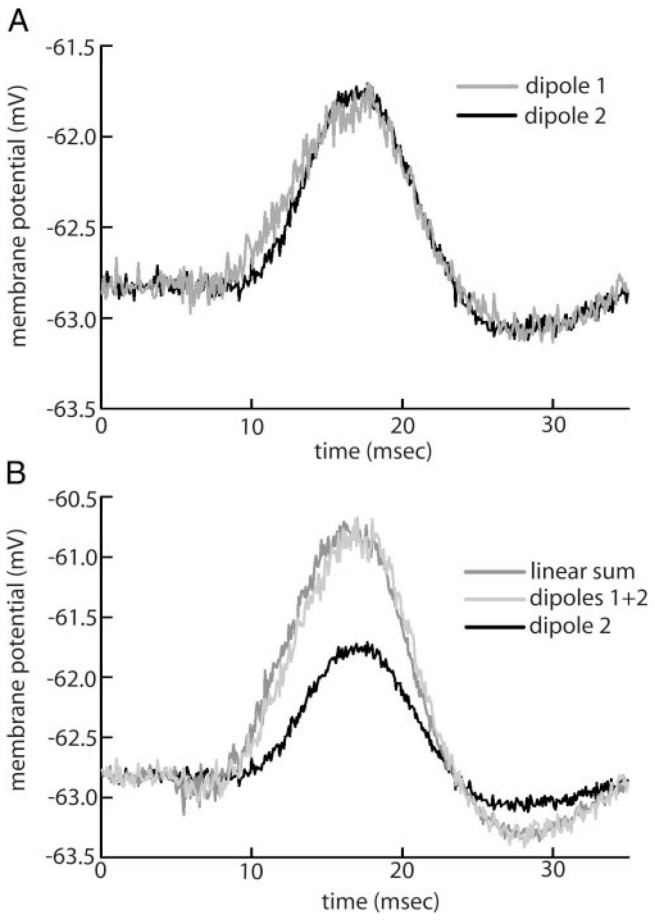

FIG. 7.

A: average compound excitatory postsynaptic potentials (EPSPs) elicited by dipole stimulation in the receptive field center of an E cell. Averages were obtained from 40 stimulus presentations. The stimulus starts at *time 0* and lasts for 4 ms. Dipole 1 (gray) elicited a compound EPSP that roughly has the same shape as the one elicited by dipole 2 (black). *B*: average compound EPSPs elicited by 1-dipole (black) vs. 2-dipole (light gray) stimulation. Linear summation of compound EPSPs occurs as seen when comparing the compound EPSP elicited by 2-dipole stimulation (light gray) to the predicted linear sum (dark gray).

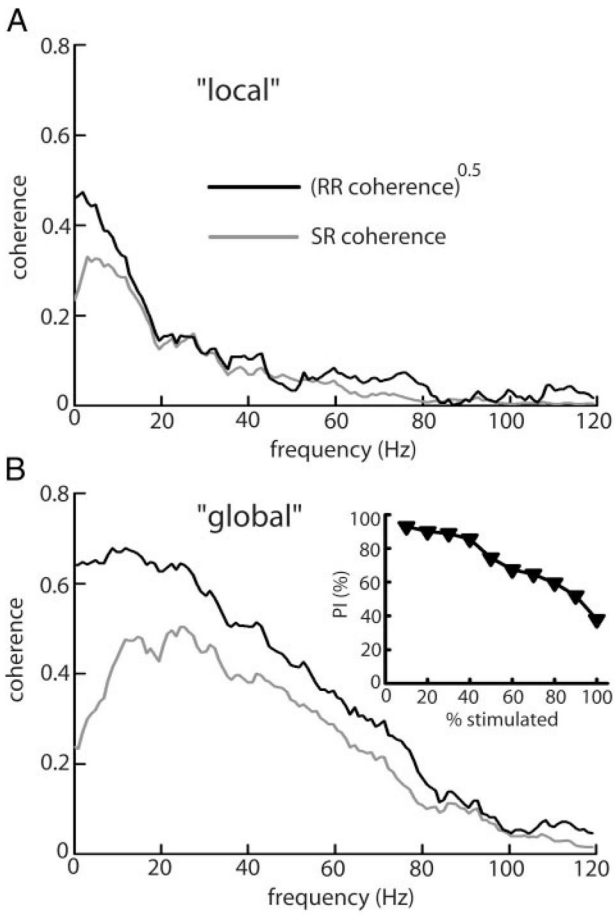

FIG. 8.

A: square rooted RR coherence (black) and SR coherence (gray) obtained with the model when 40% of receptor afferents received stimulation. Parameter values are given in the column “local” of Table 1. *B*: same quantities when 80% of receptor afferents received stimulation. Parameter values are the same as in *A* except $N_{stim} = 8$. *Inset*: performance index PI as a function of the percentage of receptor afferents receiving stimulation.

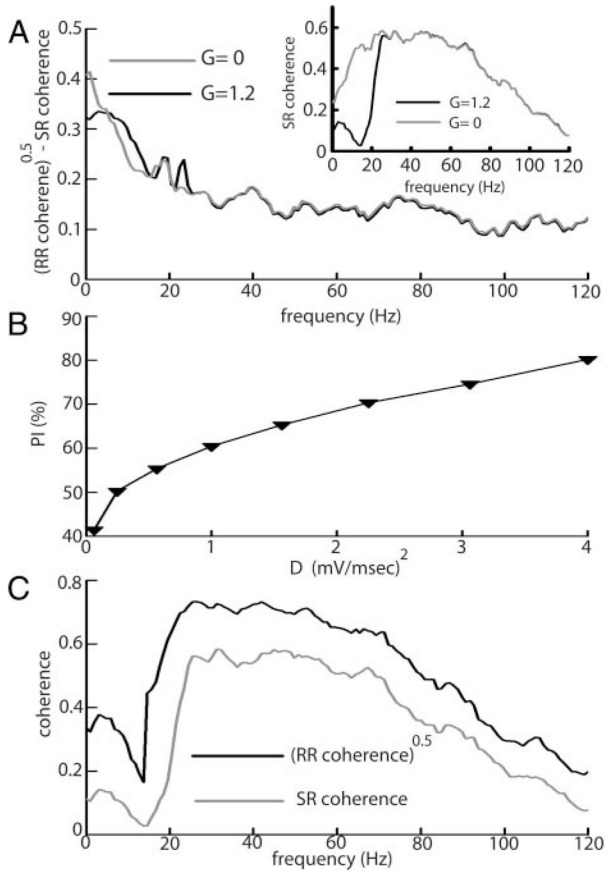

FIG. 9.

A: difference between the square rooted RR coherence and SR coherence curves with (black) and without (gray) the negative image in the model. We used G_{neg} = 1.2 mV when the negative image was present and G_{neg} = 0 mV when it was absent. *Inset*: SR coherence with (black) and without (gray) the negative image. *B*: performance index PI as a function of synaptic noise intensity *D*. Parameter values were the same as in Fig. 8*B*. *C*: square rooted RR (black) and SR (gray) coherence curves of the model under "global" stimulation. We used D = 0.01 $(mV/ms)^2$ and other parameter values are given in the column "global" of Table 1.

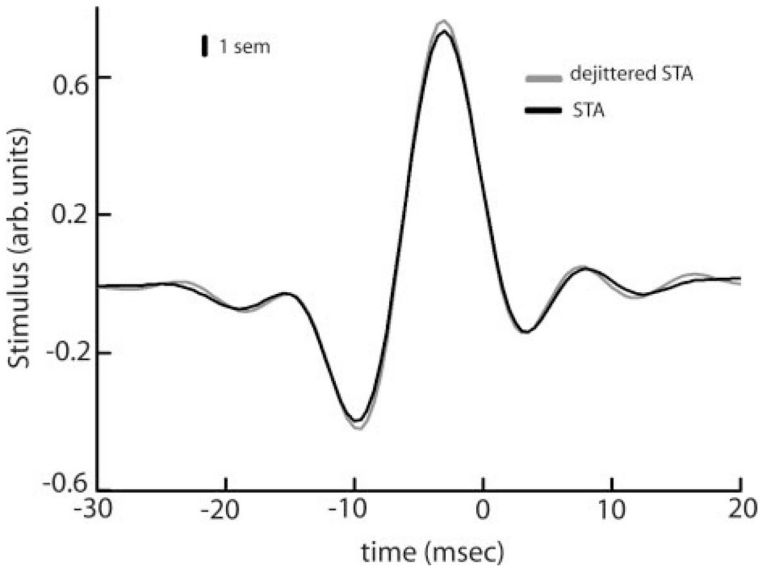

FIG. A1.

Population averaged (n = 41) raw (black) and dejittered (gray) STAs for receptor afferents under global stimulation. Vertical bars indicate 1 SE measured at 10 Hz

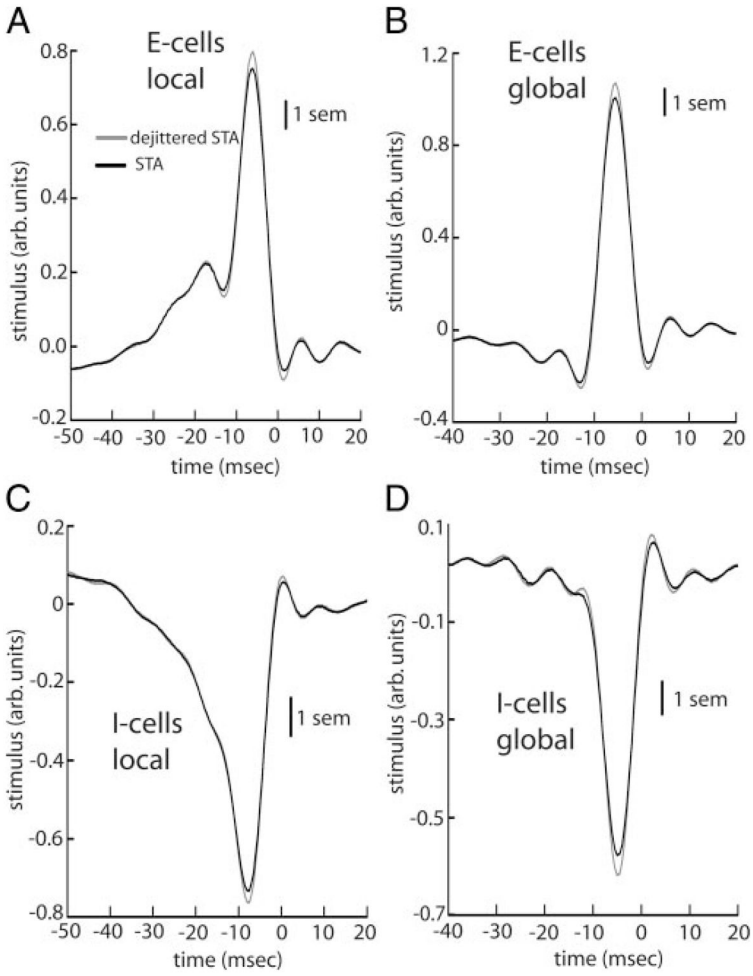

FIG. A2.

A: population averaged ($n = 27$) raw (black) and dejittered (gray) STAs for E cells under local stimulation. *B*: same quantities under global stimulation. *C*: population averaged ($n = 27$) raw (black) and dejittered (gray) STAs for I cells under local stimulation. *D*: same quantities under global stimulation. Vertical bars indicate 1 SE measured at 10 Hz.

TABLE 1

Parameter values used for the pyramidal cell model

	“Local”	**“Global”**
N_{stim}	4	8
τd, ms	50	50
C, nF	1	1
g_{leak}, μS	0.1	0.1
g_{max}, μS	5	5
E_{leak}, mV	−65	−65
E_{rev}, mV	0	0
τ, ms	1	1
D, mV/ms^2	0.09	0.01
τ_λ ms	20	20
G_{neg}	0	1.2
τ_{delay} ms	15	15

TABLE 2

Mutual information rates computed using the indirect and direct methods and the percentage ΔI of information that can be decoded linearly

	Local	Global
MI_{lower} bits/s	14.69 ± 16.51	25.15 ± 24.44**
MI_{direct} bits/s	23.10 ± 20.73	52.89 ± 37.58**
Δ*I* (%)	60.72 ± 39.05	39.05 ± 16.37**

** Statistically significant difference between the values obtained for local and global stimulation using a pairwise *t*-test at the $P = 0.01$ level with $n = 15$.

TABLE 3

PI values obtained under pharmacological blockade of feedback for local and global stimulation geometries

	Control, %	Block, %
Local	40.21 ± 15.65	27.91 ± 7.33 **
Global	25.42 ± 13.27	18.41 ± 8.70

** Significant change in PI contingent on pharmacological blockade using a pairwise *t*-test at the $P = 0.01$ level with $n = 10$.

TABLE 4

Mutual information rates computed using the indirect and upper bound methods

	MI_{upper}, bits/s	MI_{direct}, bits/s
Local	25.62 ± 25.36	23.10 ± 20.73
Global	72.93 ± 60.68	52.89 ± 37.58 *

* Statistically significant difference between the values obtained using each method using a pairwise *t*-test at the $P = 0.01$ level with $n = 15$.